Integrated modelling of precipitation during friction stir welding of 2024-T3 aluminium alloy

Emmanuel Hersent, Julian Haworth Driver, David Piot, Christophe Desrayaud

Integrated modelling of precipitation during friction stir welding of 2024-T3 aluminium alloy

E. Hersent, J. H. Driver*, D. Piot and C. Desrayaud

The microstructure and hardness profiles across a friction stir welded joint of a 2024-T3 aluminium alloy have been simulated by thermal and microstructure models. Thermal modelling is based on a semi-analytical model, which analyses the complex material flow by standard velocity fields. The precipitation model is based on classical nucleation, growth and coarsening mechanisms and can be combined with precipitation hardening laws. Applying these models in succession gives simulated hardness profiles, which have been compared to experimental hardness values after friction stir welding under equivalent conditions. The positions of maximum and minimum hardness are well reproduced, but the simulated hardness variation across the weld is less pronounced than the experimental one. The simulated microstructures in well characterised zones of the joint have been compared to previous TEM observations and shown to be generally in agreement. The results demonstrate the feasibility of making realistic hardness predictions from physically based models on a standard personal computer.

Keywords: Precipitation, Simulation, FSW, AA 2024 alloy, Hardening

Introduction

Al–Cu–Mg precipitation strengthened alloys are used in structural elements, such as the fuselage and lower wing surfaces in commercial airplanes. In recent years, joining these alloys has received a lot of interest through the invention in 1991[1] of friction stir welding (FSW), at The Welding Institute. This is a solid state welding process, which uses a rotating tool to mix material across the joint line as it advances. The advantage of this process over the classical ones is that the material does not undergo melting and so avoids solidification segregation effects (and porosity).[2] However, the weld zone is heated by intense, localised, plastic strains and friction effects, which strongly affect the precipitation state. This thermomechanical heating is of primordial importance since the strength of the alloy weld zone is directly linked to the state of precipitation. Recently, a major effort has been made to fully model this process. One of the complications, which should be noted here, is that the process is not symmetrical; the side of the weld for which the tool rotates in the same direction as the welding direction is known as the 'advancing side', and the other side, where the tool rotation is opposite, is known as the 'retreating side'. These sides see somewhat different thermal cycles and can therefore have different hardness gradients after welding.

SMS Centre, UMR CNRS 5146, Ecole des Mines de Saint Etienne, 158 Cours Fauriel, Saint Etienne 42023, France

*Corresponding author, email driver@emse.fr

Generally, complete modelling has been tackled in two steps: first with a model that predicts the temperature field as a function of the welding conditions, i.e. the advancing and rotating speeds, and second via a precipitation model, which takes the thermal field as input and then predicts the hardness profile.

For precipitation modelling of overaged aluminium alloys, the semi-empirical model proposed by Myhr and Grong in 1991,[3] has proved to be quite effective in predicting the hardness profile across a friction stir weld. It has been applied by Frigaard *et al.*[4] for AA 6082 and AA 7108, Robson and Sullivan[5] for AA 7449, and Shercliff *et al.*[6] for AA 2014. This model is based on the assumption that the number of precipitates is roughly constant. This hypothesis is acceptable for overaged alloys but cannot be applied to the underaged conditions where extensive nucleation can occur. Therefore, a model that takes into account all aspects of precipitation, i.e. nucleation, growth and dissolution, is needed. The more recent (2000) Myhr and Grong model[7] based on the Kampman and Wagner numerical framework[8] has gained a strong reputation for predicting precipitate evolution during any heat treatment. It has been applied to predict the hardness profile after gas metal arc welding of 6xxx alloys,[9] after FSW of 7xxx alloys (FSW),[10] and also after plasma arc welding of 2xxx alloys.[11] There does not appear to be a publication on modelling FSW of 2024 alloys.

The present work aims to predict the microstructure and hardness across a 2024 friction stir weld by combining a thermomechanical model developed at

Ecole des mines de Saint Etienne[12] with a slightly modified version of the precipitation model developed by Khan and Starink[13] for 2xxx alloys. These predictions will be examined in the light of detailed experimental results on FSW samples of the same alloy type, namely hardness profiles and some microstructural observations by Genevois *et al.*[14]

Materials and experimental methods

The chemical composition of the AA 2024 alloy under study is Al–4·4Cu–1·49Mg–0·22Fe–0·44Mn (wt-%). This alloy was delivered by Alcan in the form of 3·2 mm plates. The material was solution treated, quenched, stretched (2%) and aged at room temperature. The base material hardness is 137 HV.

The welding experiments were performed at the University of Louvain-La-Neuve for the European program DEEPWELD using a HERMELE 3 axis numerically controlled milling machine (UWF 1001 H) under displacement control. The dimension of the workpieces was $630 \times 450 \times 3{\cdot}2$ mm ($L \times W \times H$). The advancing and rotational speeds were continuously measured and prescribed by the controller of the milling machine. For the present study, the rotational speed was maintained constant at 400 rev min^{-1}, and two advancing rates of 100 mm min^{-1} (low welding rate) and 400 mm min^{-1} (high welding rate) were chosen. Temperature profiles were recorded during welding with type K 0·5 mm diameter thermocouples introduced at midthickness of the plates, at 8·9, 10, 12, 14 and 16 mm from the weld centreline. The 1 kg Vickers hardness values were measured 2 weeks after welding with a Zwick 3202 machine at intervals of 1 mm along the transverse section and at 2 mm from the top surface. The loading time was 30 s.

Isothermal treatments were also carried out to calibrate the hardness–microstructure relations. Each sample was immerged in a salt bath at temperatures ranging from 200 to 500°C for periods ranging from 2 s to 17 h. The samples were then water quenched. Immediately afterwards, the surface was polished, and about five hardness measurements HV1 were performed at room temperature on each sample.

Models and validation

As outlined above, modelling the hardness of friction stir welded alloys usually requires two steps: first, a calculation of the temperature field as a function of the tool advancing and rotating speeds and, second, a simulation of the precipitation evolution, from these temperature inputs, to ultimately predict the alloy strength.

It is important that the temperature field should be provided for a material element that follows a material trajectory throughout the FSW process. Based on a previous work,[12] the model used here to predict the temperature field around the pin does exactly this. The originality of the model relates to the decomposition of the material flow generated during the process by means of velocity fields classically used in fluid mechanics. The bulk material flows around the pin, so this flow could be well approximated by the classical circumventing velocity field defined for perfect fluids. In addition, the bulk material is dragged vertically by the thread of the probe. This movement is described by a vortex velocity field. Finally, the shoulder shears the material in the subsurface zones, creating a region of the weld called the 'flow arm zone'. In this region, the material flow is described by a torsion velocity field. These velocity fields can be expressed in analytical form to substantially reduce the computation times, except for the 'vortex-like' velocity field calculated by a finite element method. Using an analytical expression for the material constitutive law, it is possible to express the heat generated by the plastic strain. By adding the relevant boundary conditions, one can then resolve the classical heat equation. The model used to predict the temperature field is a more advanced version than the one previously described in Ref. 12, where the process is considered adiabatic. It differs by taking into account both heat diffusion and the heat produced by the shoulder. In particular, the surface metal is assumed to stick to the pin shoulder so that heat production results from the shearing strain in the subsurface of the shoulder. This is different from the previous method adopted in Ref. 12, which used the method of Midling and Grong.[15]

The temperature cycles simulated by the model and measured by the thermocouples are indicated on Fig. 1 for the two welding cases. The temperature measurements using thermocouples located near the weld zone during these high strain processes are somewhat uncertain: for example, the thermocouples nearest to the stir zone, at 8·9 and 10 mm on the advancing and retreating sides respectively for the welding case 100 mm min^{-1} and 400 rev min^{-1}, moved during welding. Therefore, it was not possible to get accurate measurements at these positions, but the other temperature cycles are quite reliable. The temperatures are slightly higher on the advancing side than in the retreating side. The heat production mainly depends on the plastic strain, which is greater on the advancing side because the material flow and the rotating speed are in opposite directions, so increasing the material shear. As usual, most of the work of plastic deformation is dissipated as heat.

On the advancing side, the temperatures are predicted with an error of <20°C. On the retreating side, the errors are greater, and the simulations significantly overestimate the maximum temperatures. One of the specific problems encountered here is that after welding, the simulation tends to cool the material faster than in reality. This is due to the small spatial dimension of the thermomechanical model, required to be manageable by a normal computer. If the system was bigger, one could probably allow the FSW zone to act like a stronger heat source and so reduce the overcooling by the rest of the sheet.

One may argue that an overestimation of temperature by only 20°C could have strong effects, since above roughly 350°C, the microstructure is very sensitive to very small changes in temperature. This apparent overestimation of temperature should be qualified by two points. The first point, as noted above, is that the simulation predicts shorter periods at high temperatures than in practice, so that to reach a certain level of microstructure change, higher temperature cycles are needed. The second point stems from the fact that only temperature cycles undergone by material elements are

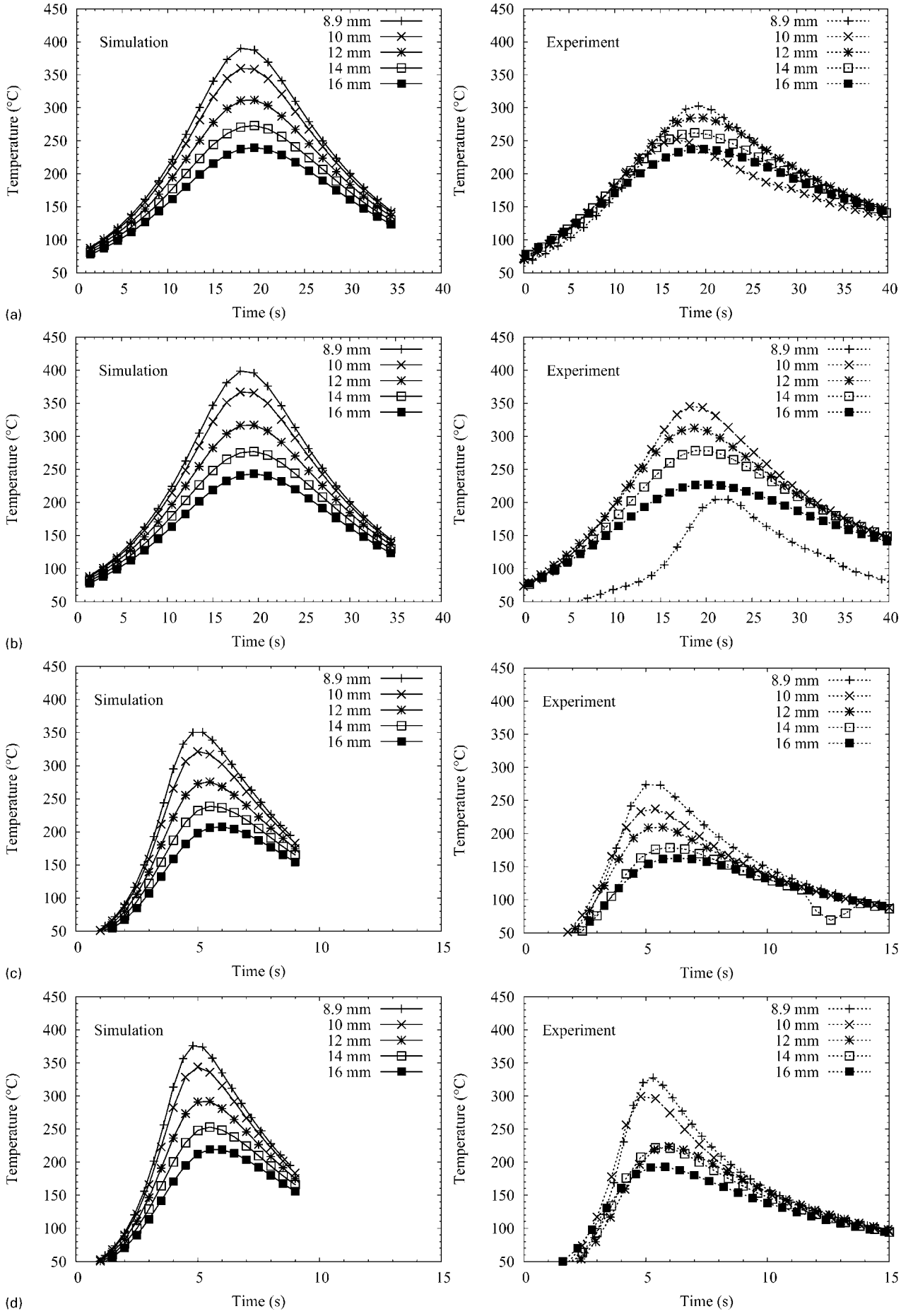

a retreating side, 100 mm min^{-1}; *b* advancing side, 100 mm min^{-1}; *c* retreating side, 400 mm min^{-1}; *d* advancing side, 400 mm min^{-1}

1 Measured (dotted lines) and predicted (solid lines) thermal cycles using analytical heat flow model developed internally[12] at different distances from weld centreline in 2024 Al alloy friction stir welded at 400 rev min^{-1}

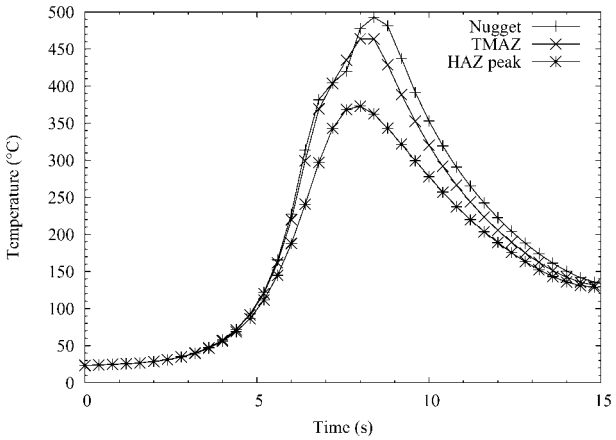

2 Heat cycles for material elements in important zones of friction stir welded joint: nugget, TMAZ and HAZ taken from peak hardness position

relevant to predict microstructure changes, and obtaining these experimental data is nearly impossible. Figure 2 shows typical heat cycles for material elements in the important zones, the nugget, the thermomechanically affected zone (TMAZ) and the heat affected zone (HAZ) on the advancing side. This is the type of data used for the precipitation model and is obtained by registering the temperature of a material element going through the predicted temperature field. Therefore, any error made in the estimated velocity field results in errors in the temperature cycle. Only qualitative agreement has been obtained between the simulated velocity fields and marker studies, which therefore only validate the main aspects of material flow during the process.[16] No quantitative comparisons are available to really evaluate the discrepancy between the experimental and estimated velocity fields and how this uncertainty influences the real temperature cycles.

The model of precipitation in 2xxx aluminium alloys developed by Kahn and Starink[13] has been adopted for the most part. Only the interfacial energy for S phase and the relation between the yield strength and hardness were modified. This model is also based on the Kampman and Wagner framework[8] and describes the nucleation, growth and coarsening rates of precipitates and calculates the particle size distribution evolution during discrete time steps. Classical nucleation and growth theory is used for the formation, growth and dissolution of particles, assuming that changes in particle size are governed by the diffusion rate of solute to or from the particle/matrix interface. The matrix composition is determined after each time step using a mean field approach.

Following classical nucleation theory, the nuclei form as a result of localised compositional fluctuations that occur statistically within the supersaturated matrix. Provided that the incubation period can be neglected, the homogeneous nucleation rate J is conveniently expressed as[17]

$$J = N_0 Z \beta^* \exp\left(-\frac{4\pi\gamma r_c^2}{3k_B T}\right) \quad (1)$$

where γ is the interfacial energy, N_0 is the number of nucleation sites per unit volume, Z is the Zeldovich non-equilibrium factor (generally taken as 0·05), β^* is the rate of atomic attachment to a growing nucleus, k_B is the Boltzmann factor and T is the temperature. The parameter r_c is the critical radius for nucleus formation, i.e. the radius for which the nucleus growth rate is zero.

In the model, the growth rate of precipitates dr/dt is evaluated by[18]

$$dr = \frac{D}{r}\frac{\overline{C} - C_i}{C_\beta - C_i}dt \quad (2)$$

where C_β is the solute concentration in the precipitates, D is the diffusion coefficient, r is the precipitate radius and C_i is the temperature dependent solute concentration at the precipitate/matrix interface.

As the size distribution of precipitates is discretised, coarsening arises naturally in the model when the growth of bigger precipitates decreases the mean solute concentration below the solute concentration at the precipitate/matrix interface of the smaller precipitates, resulting in the dissolution of the latter.

This general framework needs to be adapted for each alloy family. In aluminium alloys such as AA 2024 with a Cu/Mg atomic ratio close to one, the structures and chemistry of some (pre-) precipitates appearing during aging is controversial. Khan and Starink[13] adopted a sequence of precipitation with one metastable phase, named coclusters, and the stable phase relevant to this type of alloy, the S phase (Al_2CuMg)

$$\alpha_{ss} \rightarrow Cu - Mg \text{ co-clusters} \rightarrow S \text{ phase precipitates}$$

This precipitation sequence is consistent with the two-stage strengthening observed in this alloy with the initial stage attributed to strengthening by the Cu/Mg coclusters and the later stage attributed to strengthening by the S phase precipitates. Moreover, the shape of S phase is approximated by rods with constant aspect ratio of 10 between the length and the cross-sectional radius of the precipitates.

The Kampman and Wagner numerical framework has been applied here to S phase. The coclusters were treated with a mean radius approach described by Deschamps and Brechet.[19] This method of simultaneously treating both types of precipitates differs from that of Khan and Starink[13] who assume that heating immediately dissolves any coclusters initially present. However, and like Ref. 13, it is assumed that the coclusters form easily at room temperature so that all solutes not taken up by S phase will form coclusters, after heat treatment, up to an amount determined by their equilibrium solvus.

The challenging part of the modelling is the interfacial energy of the S phase. Generally, for 6xxx and 7xxx aluminium alloys, a constant interfacial energy is sufficient[9,10] to accurately predict the evolution of the mean radius and of the volume fraction. However, for other cases of precipitation, a more sophisticated dependence of interfacial energy is required. For example, it can depend on the radius as in the precipitation of Al_3Sc,[20] or η phase.[21] In the case of 2xxx aluminium alloys, the interfacial energy is a particularly acute problem. Thus, a constant value of the interfacial energy does not lead to the observed near constant peak strength during isothermal treatments. This incompatibility is due to the fact that if the interfacial energy is constant, the predicted strength values should increase significantly at lower temperatures due to an increase in the number of precipitates.

To introduce an improved temperature dependence in the nucleation rate, Khan and Starink[13] chose to include a temperature dependence of the interfacial energy for nucleation $\gamma_n=\gamma_{n,0}-aT^3$. However, for the later coarsening regime, these authors found that this interfacial energy was so small that it creates a long delay between nucleation/growth and coarsening. The solution they adopted to avoid this delay time was to abruptly raise the interfacial energy, by a fitting constant $\Delta\gamma$, when the nucleation rate became zero.

In the present model, the authors have followed this method of varying the interfacial energy but encountered numerical instabilities at high temperatures (about 400–500°C), related to precipitate instabilities. To solve this problem, the authors chose to increase the stability of the S phase by slightly decreasing its solubility according to the relation

$$C_{eq}=707\times10^3\ \text{mol m}^{-3}\exp\left(-\frac{38{\cdot}2\ \text{kJ mol}^{-1}}{RT}\right) \quad (3)$$

The expression for the interfacial energy was established by fitting the interfacial energy for each temperature, so that the simulated hardness evolution was close to the experimental values for a simple isothermal heat treatment. The latter consisted of heating samples of 2024-T3 in a salt bath for different times at 250–400°C (roughly the temperature range of FSW) and then quenching them before an immediate hardness measurement. The interfacial energy for nucleation was subsequently taken in a form slightly different from that of Khan and Starink as

$$\gamma_n=-9{\cdot}2020\times10^{-3}+4{\cdot}9778\times10^{-4}T-6{\cdot}0\times10^{-7}T^2 \quad (4)$$

where γ_n is in J m^{-2} and T is in K. $\Delta\gamma$ was fitted to 0·2 J m^{-2}. In addition, the interfacial energy for coclusters was taken as 2 mJ m^{-2}, and their solvus was defined according to the relation

$$C_{eq}=100\times10^3\ \text{mol m}^{-3}\exp\left(-\frac{18\ \text{kJ mol}^{-1}}{RT}\right) \quad (5)$$

The copper content in the coclusters was taken as 10%.[13]

Khan and Starink[11] also applied a precipitation hardening model to calculate the yield strength from the microstructural parameters. Following this model, the critical resolved shear stress (CRSS) due to coclusters $\Delta\tau_{cl}$ and S phase $\Delta\tau_S$ is given by

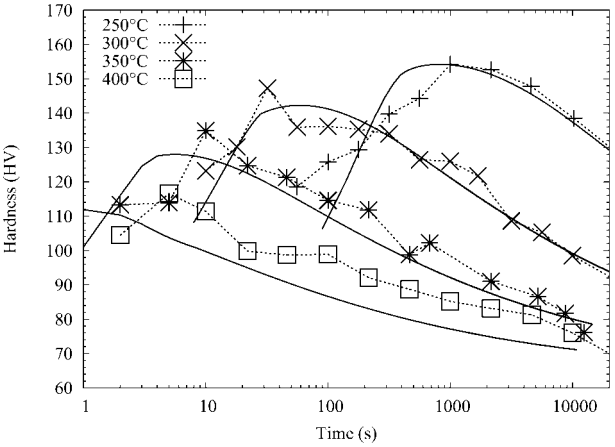

3 Experimental (dotted line) and simulated (continuous line) hardness evolution during isothermal treatments in salt bath applied to AA 2024-T3

$$\Delta\tau_{cl}=\frac{\Delta\mu}{4\pi(2)^{1/2}}f_{cl}^{1/2} \quad (6)$$

$$\Delta\tau_S=1.4\frac{0.112\mu_{Al}b}{2e_r}\ln\left(\frac{1.316e_r}{r_0}\right)\left(f_S^{1/2}+0.94f_S+2.44f_S^{3/2}\right) \quad (7)$$

where $\Delta\mu$ is the difference in the shear modulus of the matrix and the coclusters, f_{cl} and f_S are the volume fraction of coclusters and S phase, μ_{Al} is the shear modulus of aluminium, b is the magnitude of the Burgers vector and r_0 is the inner cutoff radius for the Burgers dislocation line generally considered equal to b.

The total CRSS of the grains is evaluated using the following formula

$$\Delta\tau_{tot}=\Delta\tau_{ss}+\left(\Delta\tau_{cl}^2+\Delta\tau_S^2\right)^{1/2} \quad (8)$$

where $\Delta\tau_{ss}$ is the increase in the CRSS of the grains due to the solute of the matrix, given by $\Delta\tau_{ss}=k_{ss}c$, where the constant k_{ss}=24·5 MPa at-%$^{-1}$. The total CRSS is then converted to yield strength by the linear function

$$\sigma_y=\sigma_{GB}+M\Delta\tau_{ss} \quad (9)$$

where σ_{GB} is a grain boundary strengthening (σ_{GB}=52 MPa), and the average Taylor factor M is taken as 2·6.

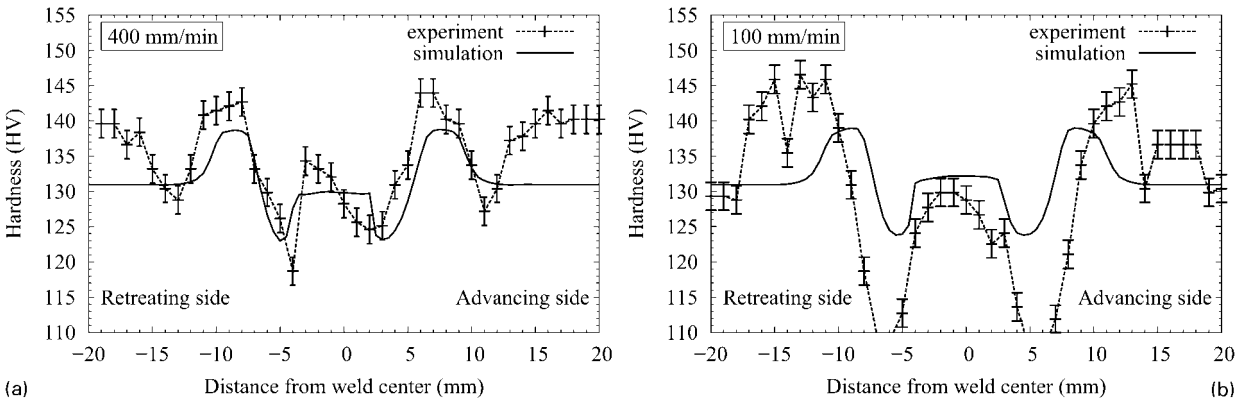

4 Experimental (dotted line) and simulated (continuous line) hardness profiles obtained on cross-section of AA 2024-T3 friction stir weld at 400 rev min^{-1} at rates of *a* 400 mm min^{-1} and *b* 100 mm min^{-1}

Following a series of tensile tests on small specimens of this alloy by Genevois,[22] the following relation between yield strength σ (MPa) and the Vickers hardness HV was adopted

$$\sigma = 3{\cdot}6774HV - 183{\cdot}25 \quad (10)$$

This relationship has been shown to be valid over a range between 110 and 160 HV.

Figure 3 presents the hardness evolution of the aged AA 2024-T3 for each temperature as a function of time. Around the peak strength, the evolutions are in good agreement, except for the 400°C series, where the simulated hardness values are systematically lower than the experimental ones by $\sim$10 HV.

Finally, a separate validation test was carried out using the same model parameters to simulate a differential scanning calorimetry (DSC) heating curve of 2024-T3.[23] This is a critical test of the model thermodynamic and kinetic parameters, particularly the interfacial energy, since the heat evolution during a DSC experiment essentially depends on precipitation and dissolution rates. The good agreement between simulated and experimental DSC curves at 20°C min^{-1} confirms that this model, despite its approximations, is capable of predicting precipitation/dissolution kinetics under non-isothermal conditions.

Results and discussion

For each material element across the joint, the temperature cycle is evaluated according to the thermomechanical model outlined above and then the quantitative precipitation behaviour of each element modelled from the temperature cycle. Using the simulated precipitate volume fraction, size and number density, it is then possible to predict the hardness profile. The resulting simulated and experimental hardness profiles are drawn in Fig. 4 for both welding conditions. First, it is clear that the general form of the spatial variations of hardness is quite well predicted by the model. Going from the base metal to the nugget centre, there is first a hardness peak at about -10 mm, then a hardness minimum around -5 mm and finally a recovery towards the base metal value in the nugget. This is the typical experimental behaviour of this alloy.[14,24] There is quite satisfactory quantitative agreement for the model and experimental hardness values developed at the higher welding rate, but the lower welding rate condition exhibits significantly greater hardness variations than expected. These two cases are discussed in more detail below.

For positions far away from the weld centre, the simulated hardness is lower than the experimental ones by $\sim$6 HV. Despite many efforts, it was difficult to adapt a strengthening model, which exactly predicts the hardness of the base metal. After the higher welding rate, there is a small drop in hardness between -14 and -12 mm, which is due to the partial dissolution of coclusters present in the base material and reveals the beginning of the heat affected zone. At these positions, the material undergoes a weld thermal treatment whose peak temperature is estimated at 200°C,[12] which is sufficient to dissolve partially the initial coclusters. No S phase is generally observed after welding for this region, so all solute released by the partial dissolution may reform coclusters, and the hardness will be close to the base metal value. However, no rehardening is observed. There can be two possibilities to explain this: one possibility is that the solid solution enrichment is too limited to enable the formation of coclusters and the second is that the lack of quenched in vacancies slows down the reprecipitation of coclusters. In the precipitation model, after the welding, the equilibrium volume fraction of coclusters was calculated at room temperature. This explains why the drop in hardness is not reproduced.

The increase in hardness between -10 and -7 mm is explained by the precipitation of small S precipitates.[14,24] The simulated peak hardness is narrower and lower than the experimental one, but the position is well reproduced.

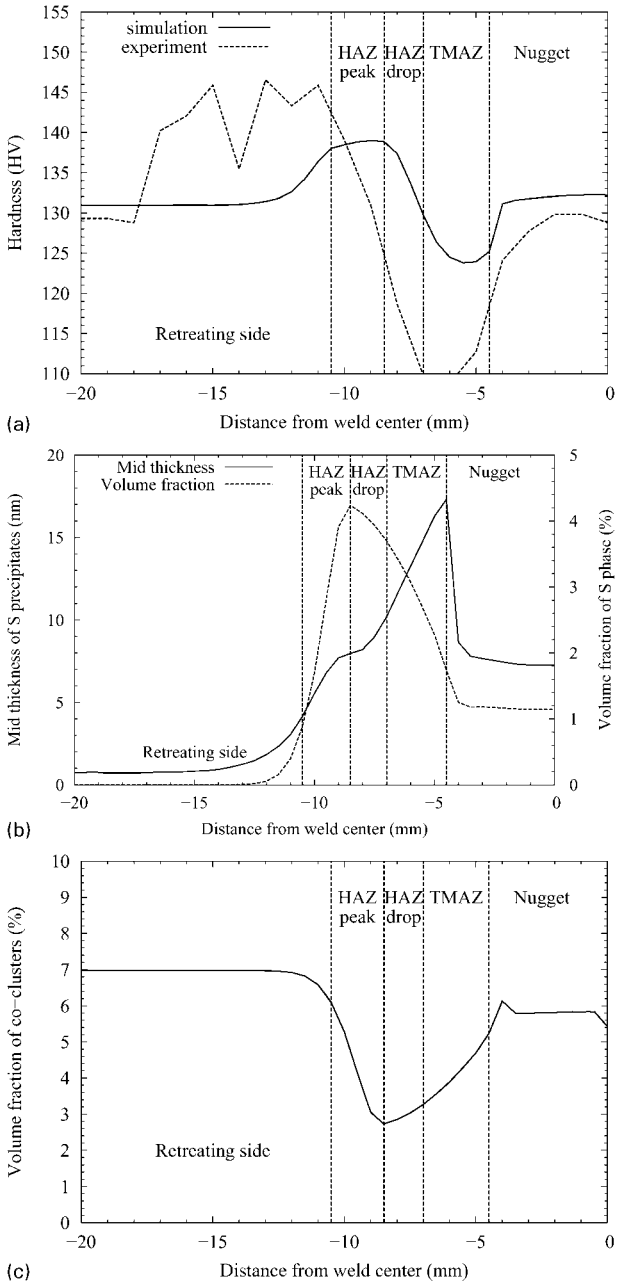

a hardness; *b* mean midthickness and volume fraction of S precipitates; *c* volume fraction of coclusters

5 Hardness and microstructural features of FSW joint from T3 initial condition: note that for comparison, cocluster volume fractions have been adjusted to Al_2CuMg composition assumed by Genevois *et al.*[14]

The more pronounced drop in hardness appearing at −5 and −3 mm is related to coarsening of the strengthening precipitates. Generally, this drop in hardness reveals the TMAZ, a region specific to FSW. At the lower welding rate, the weld temperatures are generally higher but the cooling rates are lower, roughly by a factor of 3 (Fig. 1). The lower cooling rate probably does not retain a high temperature vacancy concentration so that room temperature aging can be significantly retarded. The very high hardness drop to <110 HV at about −5 mm is tentatively attributed to the absence of room temperature aging. It seems that waiting for 2 weeks after welding is not enough for complete aging for this case of welding. For the higher welding rate, the hardness minimums are predicted further away from the weld centre than the experimental ones.

The weld nugget is characterised by a plateau on the hardness curve, close to the base metal value. The welding cycle dissolves any precipitates present in the base material and, during the cooling cycle, some coarse precipitates appear, so decreasing the available solute for precipitation during ageing. This explains why the hardness in the weld nugget is slightly lower than that in the base metal. The plateau in the simulated hardness of the weld nuggets begins at the same distance as that of the experimental one.

The precipitation model predicts the mean radius, the volume fraction of the S phase and the volume fraction of coclusters across the welds. Their evolutions for the retreating side are given in Fig. 5. These values can be compared to the ones measured in a friction stir welded 2024-T3 by Genevois *et al.*[14] and which are summarised in Table 1. The volume fraction was measured by a combination of DSC and small angle X-ray scattering (SAXS) techniques and the precipitate size by combining TEM and SAXS. It should be pointed out that the weld examined by Genevois was made with slightly different conditions (an advancing speed of 100 mm min^{-1} and a rotating speed of 800 rev min^{-1}). These experimental microstructures were therefore compared with the authors' simulations for the welded joint with the closest conditions: 100 mm min^{-1} and 400 rev min^{-1}. Despite the higher experimental welding rate, the hardness values in the different regions of the weld are close, only the positions of the maximum and minimum are displaced. One can therefore expect the simulated microstructures to be similar to the measured ones. According to Ref. 14, the HAZ of a 2024-T351 friction stir welded exhibits a strong microstructure gradient, here divided into three parts: partial dissolution, peak strength named HAZ peak and the drop in hardness (HAZ drop). Only the latter two parts are assessed in terms of the simulated hardness profile because of the authors' inability to reproduce the partial dissolution of coclusters.

In Table 1, it is seen that the simulated volume fraction of coclusters in the base metal is close to, but slightly higher than, that of the experimental ones, the difference being attributed to the fact that the simulation gives the equilibrium quantities. In the HAZ peak, as already pointed out, the decrease in the volume fraction of coclusters is underestimated due to kinetic factors. However, the evolution of the S phase in the HAZ peak is in agreement with the experiment, although the thickness of the simulated S precipitate is slightly greater. In the HAZ drop, the simulated volume fraction of coclusters is 2% higher than that of the experimental one as in the base material zone. The simulated evolution of the volume fraction of S phase is less than the experimental one, and the simulated thickness is twice the experimental value.

In the TMAZ, the simulated volume fraction and mean radius of S phase are in good agreement with the experimental ones. The volume fraction of coclusters increases by roughly 3%, whereas the experimental one increases by 2%.

From the border of the weld nugget, the experimental volume fraction of coclusters increases sharply to reach the volume fraction level at the centre of the nugget, whereas the simulated volume fraction already reaches this level at the end of the TMAZ. The simulated volume fraction of S phase matches quite well with that of the experimental ones. The simulated mean radius is largely underevaluated. Precipitates thicker than 100 nm have also been observed in the weld nugget.[25] One explanation is that the thermomechanical model cools down the weld more rapidly than in practice so that the precipitates do not have time to grow. This underevaluation of the thickness does not really have a great influence on the hardness. If the simulated thickness had the experimental value, the hardness would only decrease by 5 HV. The small influence of an error in the mean radius is due to the relatively low value of the volume fraction.

Conclusions

The FSW process for 2xxx aluminium alloys has been completely modelled using a thermomechanical and a

Table 1 Summary of microstructure measurements made by Genevois *et al.*[14] for retreating side of 2024-T3 friction stir weld and comparison with simulated microstructures*

		Volume fraction, %		Average thickness, nm	
Weld regions	Nature of the precipitates	SAXS/DSC	Simulation	TEM/SAXS	Simulation
Base metal	Coclusters	5	7	…	…
HAZ peak	Coclusters	4·8–1	6–3	…	…
	S phase	0–3	1–4	8	8–16
HAZ drop	Coclusters	~1	~3	…	…
	S phase	3·2–4	~4	8–11	16–20
TMAZ	Coclusters	1–2·8	3–5·8	…	…
	S phase	4–3	4–1·8	11–30	20–34
Nugget	Coclusters	3·75	5·8	…	…
	S phase	1	1·2	Up to 62	14

*For comparison, the cocluster volume fractions have been adjusted to the Al_2CuMg composition assumed by Ref. 14.

precipitation model. With these two models, it is possible to simulate the hardness profile and the evolution of relevant parameters of the strengthening precipitates across the welds. The simulations have been compared to the experimental hardness measurements. The positions of the minimum and maximum peaks of the hardness profiles are well reproduced. However, the simulated variation in hardness is less than that in the experimental one: the maximum is not as high and the minimum not as low. The simulated microstructures have also been compared to experimental values of precipitate size and volume fraction measured on FSW welds of the same alloy by Genevois *et al.*[14] Generally, the microstructure is well reproduced, except for the weld nugget where the mean radius of the S phase is underestimated because of a higher cooling rate in the thermomechanical model.

A number of improvements to the current models can be made. The first is to better simulate the heating cycles during FSW; an improved model of FSW based on the current semi-analytical method is presently being completed.[26] Another would be its extension to other alloy systems. The present metallurgical model is limited to Al–Cu–Mg alloys with a Cu/Mg atomic ratio close to one. Based on the present work, it is quite feasible to explore the effect of modifying the alloy composition on the hardness profile across the welds. Such a tool could be useful to optimise the weld properties. Finally, a natural continuation of this work is to simulate the overall mechanical behaviour of the weld by predicting the strain hardening in each region of the weld. It could also be useful to predict the necking location.

Acknowledgements

The authors wish to thank the European community for its financial support to the Detailed Multi-physics Modelling of Friction Steer Welding (DEEPWELD) project in the context of which this work was performed. The DEEPWELD project (AST4-CT-2005-516134) is a 36 month Specific Targeted Research Project co-funded by the 6th Framework Programme of the European Community. (This publication reflects only the authors' views; the European Community is not liable for any use that may be made of the information contained therein.) The authors also wish to thank the University of Louvain-La-Neuve for carrying out the welding.

References

1. W. M. Thomas, E. D. Nicholas, J. C. Needham, M. G. Murch, P. Temple-Smith and C. J. Dawes: 'Friction stir butt welding', International patent application PCT/GB92, patent application no. GB9125978·8, 6, December 1991.
2. P. L. Threadgill, A. J. Leonard, H. R. Shercliff and P. J. Withers: *Int. Mater. Rev.*, 2009, **5**, 49–93.
3. O. R. Myhr and Ø. Grong: *Acta Mater.*, 1991, **39**, 2693–2702
4. Ø. Frigaard, Ø. Grong and O. T. Midling: *Metall. Trans. A*, 2001, **32A**, 1189–1200.
5. J. D. Robson and A. Sullivan: *Mater. Sci. Technol.*, 2006, **22**, 146–152
6. H. R. Shercliff, M. J. Russel, A. Taylor and T. L. Dickerson: *Méc. Ind.*, 2005, **6**, 25–35.
7. O. R. Myhr and Ø. Grong: *Acta Mater.*, 2000, **48**, 1605–1615.
8. R. Wagner and R. Kampmann: 'Materials science and technology – a comprehensive treatment', 213–303; 1991, Weinhem, VCH.
9. O. R. Myhr, Ø. Grong, H. G. Fjær and C. D. Marioara: *Acta Mater.*, 2004, **52**, 4997–5008.
10. N. Kamp, A. Sullivan, R. Tomasi and J. D. Robson: *Acta Mater.*, 2006, **54**, 2003–2014.
11. I. N. Khan, M. J. Starink, I. Sinclair and S. C. Wang: *Mater. Sci. Technol.*, 2008, **24**, 1411–1418.
12. P. Heurtier, M. J. Jones, C. Desrayaud, J. H. Driver, F. Montheillet and D. Allehaux: *J. Mater. Process. Technol.*, 2006, **171**, 348–357.
13. I. N. Khan and M. J. Starink: *Mater. Sci. Technol.*, 2008, **24**, 1403–1410
14. C. Genevois, A. Deschamps, A. Denquin and B. Doisneau-cottignies: *Acta Mater.*, 2005, **53**, 2447–2458.
15. O. T. Midling and Ø. Grong: *Acta Metall. Mater.*, 1994, **42**, 1595–1609.
16. A. P. Reynolds: *Scr. Mater.*, 2008, **58**, 338–342.
17. C. Zener: *J. Appl. Phys.*, 1949, **20**, 950–953.
18. J. B. Zeldovich: *Acta Physiocochim. USSR*, 1943, **18**, 1–22.
19. A. Deschamps and Y. Brechet: *Acta Metall.*, 1998, **47**, 293–305.
20. J. D. Robson, M. J. Jones and P. B. Prangnell: *Acta Mater.*, 2002, **51**, 1453–1468.
21. C. Sigli: *Mater. Sci. Forum*, 2006, **519–521**, 321–326.
22. C. Genevois: 'Genèse des microstructures lors du soudage par friction malaxage d'alliages d'aluminium de la série 2000 & 5000 et comportement mécanique résultant', PhD thesis, Institut National Poytechnique de Grenoble, Grenoble, France, 2004.
23. E. Hersent, J. H. Driver and D. Piot: *Scr. Mater.*, 2010, **62**, 455–457.
24. M. J. Jones, P. Heurtier, C. Desrayaud, F. Montheillet, D. Allehaux and J. H. Driver: *Scr. Mater.*, 2005, **52**, 693–697.
25. P. Heurtier: 'Etude et simulation de soudures obtenues par procédé de frottement-malaxage (FSW) sur des alliages d'aluminium de la série 2000', PhD thesis, École des mines de Saint-Étienne, Saint-Étienne, France, 2004.
26. D. Jacquin, B. de Meester, A. Simar, D. Deloison, F. Montheillet and C. Desrayaud: *J. Mater. Process. Technol.*, 2010, doi 10.1016/j.jmatprotec.2010.08.016.